JOURNAL OF AIRCRAFT
Vol. 44, No. 1, January–February 2007

Aerodynamic Performance of a Biplane Micro Air Vehicle

Jean-Marc Moschetta* and Chinnapat Thipyopas†
Ecole Nationale Supérieure de l'Aéronautique et de l'Espace, 31055 Toulouse, France

DOI: 10.2514/1.23286

The present paper addresses the problem of improving the aerodynamic performance of a fixed-wing micro air vehicle under stringent maximum size constraints. Monoplane wing planforms are compared with biplane concepts using low-speed wind-tunnel measurements and numerical calculations including viscous effects. A parametric study of the effect of various geometrical parameters such as aspect ratio, gap, stagger, and wing planforms has been carried out in order to optimize a biplane micro air vehicle configuration in the low-Reynolds regime. Finally, wind-tunnel measurements including the influence of propellers indicate that biplane micro air vehicle configurations can drastically increase the overall aerodynamic performance over the classical monoplane fixed-wing concept.

Nomenclature

AR	=	aspect ratio
B	=	maximum dimension
b	=	wingspan
C_D	=	drag coefficient
C_{Di}	=	induced drag coefficient
C_{D0}	=	drag coefficient at zero lift
C_f	=	mean skin friction coefficient
C_L	=	lift coefficient
$C_{L\text{cruise}}$	=	lift coefficient at cruise condition
$C_{L\max}$	=	maximum lift coefficient
$\bar{c}$	=	mean wing chord
c_f	=	local skin friction coefficient
D	=	total drag force
D_f	=	skin friction drag force
D_i	=	induced drag force
G	=	vertical distance between biplane wings
k	=	induced drag factor
l	=	pitching moment arm
L	=	lift force
L/D	=	lift-to-drag ratio
P	=	motor power
p	=	yawing/rolling moment arm
q	=	dynamic pressure, $q = \frac{1}{2}\rho_\infty V_\infty^2$
r	=	drag ratio, $r = D_i/D$
Re	=	Reynolds number based on mean wing chord
Re_u	=	Reynolds number for a unit length
S	=	wing area
s	=	parasite drag factor
T	=	thrust
V	=	flight speed
W	=	weight
α	=	angle of attack; deg
β	=	biplane interference factor
ϵ	=	designates an error quantity
ρ	=	air density
σ	=	interference factor in Prandtl biplane theory
υ	=	kinematic viscosity

Subscripts

Bi	=	biplane
Mo	=	monoplane

Presented as Paper 4613 at the 23rd AIAA Applied Aerodynamics Conference, Toronto, Canada, 6–9 June 2005; received 20 February 2006; revision received 22 May 2006; accepted for publication 22 May 2006.

*Professor of Aerodynamics, Laboratoire en Mécanique des Fluides, Energétique et Propulsion; also ONERA, 31055 Toulouse, France; moscheta@supaero.fr. Member AIAA.

†Graduate Student, Laboratoire en Mécanique des Fluides, Energétique et Propulsion; thipyopa@supaero.fr.

Introduction

Micro air vehicles (MAV) are essentially characterized by very stringent dimensional constraints (typically 6–8 in or 15–20 cm) which the need suggests to maximize the wing area in order to produce a significant lift force. This strategy classically leads to fairly low aspect-ratio wings (typically between 1 and 1.4), such as the *Black Widow* [1], which generally produce high induced drag in cruise conditions. Previous wind-tunnel measurements [2–4] have shown that the induced drag may represent up to 70 to 80% of the overall aerodynamic drag at cruising speed, whereas the induced drag for a well-designed classical airplane typically represents about 50% of the total drag. The main objective of this paper is to optimize the aerodynamic performance of a MAV prototype not only at high cruise speed but also at low speed when the vehicle is slowly circling over its target in order to capture and transmit a clear image to the pilot.

The major effect of biplane wings is roughly to divide the induced drag by a factor of 2 at the price of a parasite drag increase. The ideas considered in this paper are to assess the possibility of applying the classical concept of biplane wings to MAV configurations. This present optimization process consists of minimizing the total aerodynamic drag force while keeping constant the following parameters: 1) cruising speed V, 2) maximum dimension B, 3) lift force (or total weight W). In this study, the overall maximum dimension is equal to 20 cm, which is consistent with previous monoplane MAVs developed at Ecole Nationale Supérieure de l'Aéronautique et de l'Espace (SUPAERO). The lift force should balance a total weight of 80 g. This value has been chosen so as to include: airframe, batteries, motor, propeller, receiver, servos, automatic pilot, and payload (video camera and transmitter). Finally, the cruising speed is chosen in order to fly near the maximum lift-to-drag ratio condition, with a sufficient maneuverability margin. For fixed-wing MAVs, the total drag coefficient can be written as

$$C_D = C_{D_0} + kC_L^2 \tag{1}$$

whereas present experimental studies carried out on monoplane wings (see Table 1, below) indicate that $C_{D_0} \approx 0.03$ and $k \approx 0.3$ correspond to optimized planforms. The lift-to-drag ratio

$$L/D = \frac{C_L}{C_{D_0} + kC_L^2} \tag{2}$$

is at a maximum for $C_L = (C_{D_0}/k)^{1/2} \approx 0.316$ and $(L/D)_{\max} = 0.5(kC_{D_0})^{-1/2} \approx 5.27$. The corresponding cruising speed is then equal to $V \approx (2W/\rho S C_L)^{1/2} \approx 11.4$ m/s. Another desirable cruise

Table 1 Comparison of wings aerodynamic performances

Planform	Area (cm^2)	Λ	C_{D0}	K	$(L/D)_{\max}$	$(L/D)_{\text{cruise}}$	α_{cruise} (deg)	$C_{L\max}/C_{L\text{cruise}}$
Zim	264	1.14	0.053	0.54	4.04	4.02	9.0	3.05
Zim 2	173	2.32	0.042	0.33	5.11	4.72	8.8	1.43
InvZim	264	1.14	0.049	0.58	3.97	3.79	7.4	2.40
InvZim 2	173	2.32	0.034	0.35	4.76	4.62	7.4	1.46
Plaster	245	1.40	0.041	0.36	4.98	4.86	6.4	2.21
Plaster 2	166	1.80	0.035	0.29	5.47	5.03	7.0	1.88
Drenalyn	273	1.26	0.053	0.42	4.72	4.69	7.2	3.07
Drenalyn 2	173	2.32	0.038	0.30	4.81	4.65	7.6	1.43
Trapezoidal	225	1.00	0.048	0.51	4.24	4.09	7.8	2.79
Swept 25	147	2.50	0.044	0.35	5.19	4.72	11.0	1.27
Circle	314	1.27	0.059	0.38	3.02	2.97	8.0	2.61
Square	200	1.00	0.047	0.59	2.95	2.21	11.5	1.38

speed is the speed that minimizes the motor power P

$$P = TV = DV = \frac{1}{2}\rho V^3 S C_{D_0} + \frac{2kW^2}{\rho SV} = a_1 V^3 + \frac{a_2}{V} \qquad (3)$$

P is minimum for $V = (a_2/3a_1)^{1/4} \approx 8.6$ m/s. Therefore, in the following, an average nominal speed of 10 m/s has been selected to compare the different wing configurations.

Finally, another requirement for suitable MAV wings is that the maximum lift force should be sufficient for maneuverability and for allowing slow-flight phases when video-transmission is performed. Therefore, MAV wings should provide high lift coefficients in spite of the low-Reynolds regime.

Optimization of Monoplane Wings

Wing Models

Previous experimental studies [2–4] have been confirmed and augmented by the present investigation in order to determine the best monoplane wing planform suitable for fixed-wing MAVs. Figure 1 illustrates a selection of wing models of varying planform shapes. All wing models were made of composite Fiberglass resin to fit into a 20 cm-wide disk. Three layers of fine Fiberglass type and two thick Fiberglass layers were applied so that no deformation could be observed at 10 m/s. All models had a thickness of 1 mm and a leading edge radius of about 0.5 mm. The small relative thickness used here was selected because thin airfoils provide better aerodynamic performance in the low-Reynolds regime. The trailing edge was linearly tapered over a length of 1 mm. For each model, the 5%-camber *Göttingen 417a* camberline [5] has been reproduced along the wing root chord. An additional 16 swept wing models have been previously tested [6], including various sweepback angles, aspect ratios, and taper ratios. Only the two best performing swept-back wings have been retained in the present study, "Swept 25," sweep angle of 25 deg, aspect ratio 2.5 and taper ratio 0.6 and "trapezoidal," no swept, aspect ratio 1 and taper ratio 0.6. The "Zimmerman" [7] and "inverse Zimmerman" planform shapes are formed by joining two half-ellipses at either the quarter-chord or the three-quarter-chord location. The Plaster wing planform shape is formed by joining a half-ellipse and a rounded-corner rectangle at the quarter chord and the "Drenalyn" is formed by cutting off a three-quarter ellipse in order to fit into the disk.

Experimental Setup

Experimental measurements have been done in a closed-loop low-speed wind-tunnel at the Aerodynamics Laboratory of SUPAERO (Fig. 2). The test section is 70 cm long with a square cross-sectional area of 45 × 45 cm. This wind tunnel has a contraction ratio of 6.2 to 1 and the flow speed can be adjusted by controlling the motor speed. The maximum flow speed is 45 m/s. Speed measurement is performed through a Pitot pressure tube located at the beginning of the wind-tunnel test section. Both total and static pressure tubes are connected with a pressure transducer to measure the actual dynamic pressure. A series of grids at the beginning of the contraction part gradually splits and damps vortical structures so that the turbulence intensity of the incoming flow is reasonably low (~1%).

A three-component balance mounted externally below the wind-tunnel test section was initially used in the study. However, its accuracy proved to be insufficient for MAV application. Indeed, one difficulty to experimentally measure aerodynamic forces and moments applied to MAVs is the balance precision [8]. To achieve better measurement accuracy, a new 5-component balance has been designed and fabricated (Fig. 3). A computer-controlled stepper motor is used for varying the model angle of attack from −8 to +30 deg. Models are mounted on three struts whose drag has been carefully measured as a function of the angle of attack. The balance is assembled from five single point load cells (precision ±0.002 N

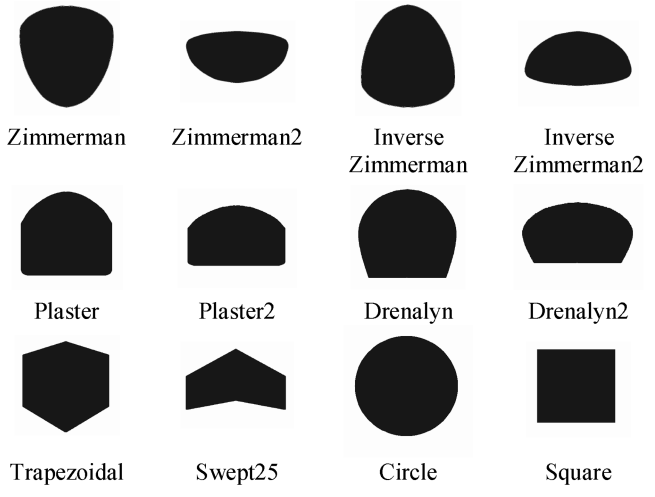

Fig. 1 Wing models.

Fig. 2 Wind-tunnel test section.

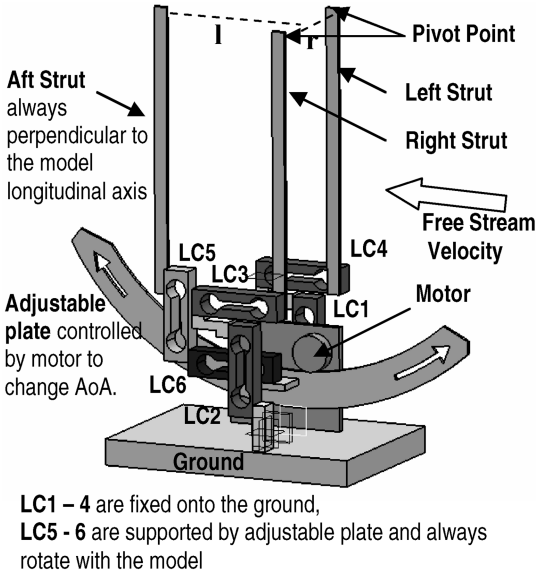

Fig. 3 New 5-component high-accuracy balance for MAV's.

through the data acquisition system) which have nonlinearity and nonrepeatability 0.02% of rated output. The data are obtained by the average values from 1000 measurements at an acquisition rate of 1 kHz.

Four load cells, two in the x direction (drag force LC1&2) and two in the z direction (lift force LC3&4), are fixed onto the ground and support the front (left and right) struts. The LC5-6 load cells supported by the adjustable plate can rotate with the model so that the center of rotation is at the pivot point when the angle of attack is varied. LC6, which is always perpendicular to the model longitudinal axis, is used to measure the normal force which can be transformed into the pitching moment through multiplication of moment arm l. The LC5 is used to measure the aft strut's drag and contributes to correct the model drag measurement. The aerodynamic forces and moments are then calculated by

$$\text{lift} = F_{LC3} + F_{LC4} + F_{LC6} \cdot \cos\alpha \tag{4}$$

$$\text{drag} = F_{LC1} + F_{LC2} + F_{LC6} \cdot \sin\alpha \tag{5}$$

$$\text{pitching moment} = F_{LC6} \cdot l \tag{6}$$

$$\begin{aligned} \text{rolling moment} &= (F_{LC3} - F_{LC4}) \cdot p, \\ \text{yawing moment} &= (F_{LC2} - F_{LC1}) \cdot p \end{aligned} \tag{7}$$

The main advantage of this new aerodynamic balance is that the pitching moment only involves two measured quantities, a force from load cell LC6 and moment arm l, without any additional term depending on the angle of attack as for a standard fixed-strut balance. Using Kline and McClintock's method, the uncertainty values in pitching moment for the new balance is:

$$\text{pitching}_{\text{New}} = [\varepsilon_{LC6}^2 + \varepsilon_l^2]^{1/2} \tag{8}$$

The validation of the new aerodynamic balance was done by known mass calibration. Each measurement is the mean average over 1000 measured values. The resulting accuracy in force measurement was found to be ± 0.005 N. and the accuracy in pitching moment is ± 0.02 N cm for a moment arm l equal to 10 cm. This accuracy can be further improved if the moment arm is reduced. The present force balance gives much higher accuracy if compared with the standard previous balance that had an accuracy of about ± 0.02 N in force. The performance of the new balance is very satisfactory when compared with the 0.01 N force-resolution and 0.05 N cm moment resolution reported by Pelletier and Mueller [4] but still less accurate than Kochersberger's [9].

The signals from the strain gauges were measured with very sensitive instrumentation using a full Wheatstone bridge configuration. The output signals were read with an instrumentation amplifier circuit, with available gains from 1 to 1000. The amplified analogue signals were sent to the computer and converted using a six-channel converter. Before measuring any aerodynamic force or moment with the balance, the amplifier gains were adjusted to minimize the error. The dynamic pressure was measured at zero angle of attack to set the incoming flow speed at 10 m/s.

The drag force from the three struts without the presence of the wing model was measured before each model test. Then, the model drag was obtained by

$$D_{\text{model}} = D_{\text{total}} - D_{\text{struts}} \tag{9}$$

To account for the actual interaction between the struts and the model, the drag of the struts *in the presence of* the model was also measured and compared with the struts drag without model. The wing model was then supported by another strut from the top of the wind-tunnel test section. Several angles of attack were compared and it was found that the struts drag in both cases was almost identical (less than 1% error in the struts drag).

A solid-blockage correction combined with Maskell's wake blockage correction as described in [10] have been applied to all measured quantities.

Discussion of Results

All wing models were measured at a constant flow speed of 10 m/s so as to produce a nominal lift force corresponding to 80 g. Although the different models had different wing areas, all aerodynamics coefficients have been calculated using a common reference surface corresponding to the 20-cm-diameter disk area. Therefore, direct drag force comparison can be obtained from the lift-to-drag ratio at cruise speed as illustrated in Table 1. Furthermore, the last column of Table 1 gives the ratio of maximum lift to cruise lift, which gives an indication of the maneuverability margin and the capability to sustain low-speed flight. It appears from Table 1 that the circular planform which maximizes the wing area produces poor aerodynamic performance in terms of drag force at cruise conditions, whereas the sweepback wing achieves a high lift-to-drag ratio at cruise conditions but fails in terms of maximum lift. Finally, the most promising candidates for monoplane wings are the Zimmerman [3] and the Plaster planforms which both provide relatively high values of the cruise lift-to-drag ratio and a sufficient maneuverability margin. The choice for the most suitable aspect-ratio results from a tradeoff between cruise lift-to-drag ratio and maximum lift. On Fig. 4, the lift-to-drag ratio of three wings is plotted as a function of the lift coefficient based on the actual wing surface. The three wings are a circular planform wing ($AR = 1.27$) and two elliptical planform wings ($AR = 1.5$ and $AR = 1.9$). It can be observed that reducing the mean chord for a given overall maximum size is beneficial to the maximum lift-to-drag ratio. The lift-to-drag ratio at different aspect ratios is achieved at approximately the same value of the lift coefficient ($C_L \cong 0.45$). However, the maximum lift tends to decrease as the aspect ratio increases. If the aspect ratio were further increased, the maximum lift-to-drag ratio would be obtained at a lift coefficient too close to stall. A practical rule in order to maintain a sufficient safety margin is to ensure that the maximum lift coefficient is at least twice as high as the cruise lift coefficient. Therefore, a maximum value of 1.9 should be adopted for monoplane MAV wings.

In the present calculation, the maximum dimension is assumed to be the wingspan ($B = b$). For a steady level flight, forces applied to an airplane are in equilibrium. Taking into account the definition $AR = b^2/S$ and utilizing the expression for the drag coefficient $C_D = C_{D0} + C_L^2/\pi AR$, the equations of equilibrium of an airplane in the vertical and horizontal direction, respectively, are

$$W = qC_L S = qC_L b^2/AR \tag{10}$$

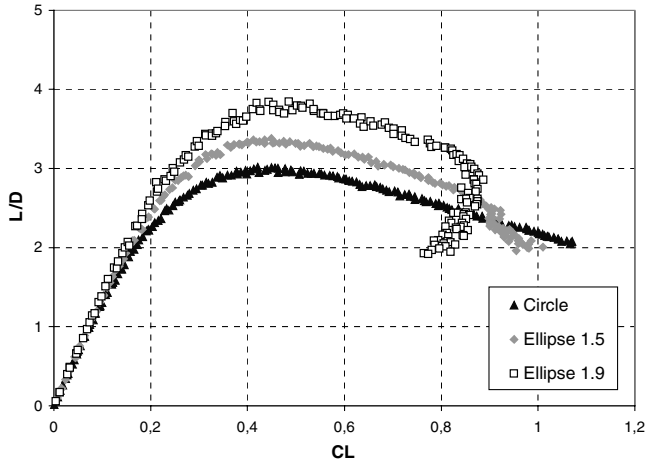

Fig. 4 Influence of the lift-to-drag ratio.

$$T = qC_D S = q\lfloor SC_{D_0} + SC_L^2/\pi AR \rfloor \tag{11}$$

If W, q, and b are constant, it follows from Eq. (10) that C_L/AR is constant. From Eq. (11), at constant q, a minimum required thrust corresponds to the minimum sum of skin friction drag and induced drag. Because $S = b^2/AR$, the term related to the induced drag can be written as

$$\frac{SC_L^2}{\pi AR} = \frac{b^2}{\pi}\left(\frac{C_L}{AR}\right)^2 \tag{12}$$

Since b is fixed and the ratio C_L/AR is constant, the induced drag will not vary when the aspect ratio is increased. This is due to the fact that when reducing the mean chord, the wing area is accordingly reduced which implies an increase of the angle of attack to maintain a constant lift force. Therefore, the intrinsic reduction of the induced drag due to a greater aspect ratio is exactly balanced by the increase of angle of attack. For a laminar boundary layer, the term related to skin friction drag can be presented as [11]

$$SC_{D0} = 2SC_f = 2S\frac{h}{Re^{1/2}}, \qquad h \cong 1.328 \tag{13}$$

Using the Reynolds-number definition and because $S = b\bar{c}$, where $\bar{c}$ is a mean aerodynamic chord, after rearrangements, Eq. (13) can be written as

$$SC_{D_0} = \frac{2h}{Re_u^{1/2}} b\sqrt{\bar{c}} = gb\sqrt{\bar{c}} \tag{14}$$

where g is a constant depending on Reynolds number for a unit length. It follows from Eq. (14) that for a constant wingspan skin friction drag decreases as the mean aerodynamic chord decreases. As a conclusion, all monoplane wings flying at a given speed and producing the same lift force for a fixed span will virtually produce the same induced drag force whatever the aspect ratio is. However, the total drag will be reduced when reducing the mean wing chord, provided that the resulting cruise lift is sufficiently far from stall. This paradox has been the major source of inspiration for considering strategies in which the aspect ratio is artificially increased whereas the wing area is not reduced. This is precisely the case for winglets [12] and for the biplane configuration [6,13].

Monoplane vs Biplane MAVs

Fixed-Wing MAV Conceptual Design

The advantage of using biplane wings for MAVs can be understood by considering that the major design constraint for such vehicles is the overall maximum size. Instead of considering a 20-cm-wide disc and trying to optimize a monoplane wing planform, the idea is to take advantage of the third dimension by doubling the wing surface such that it fits into a 20-cm-diameter sphere. For a fixed total weight and a constant cruise speed, doubling the wing area means dividing the wing load by a factor of 2. Each wing will then produce an induced drag proportional to the square of the lift force. The sum of both induced drag forces is then roughly half of the total induced drag produced by a monoplane wing of identical wing area and maximum overall size.

Table 2 illustrates that for a given span, a higher aspect-ratio monoplane wing yields a smaller total drag due to a smaller wetted area. Yet, for a fixed weight, the induced drag is not changed when the chord is reduced. This is due to the fact that the angle of attack must increase to compensate the wing area reduction. However, when reducing the wing area, the lift at cruise conditions may become too close to the maximum lift, which results in poor maneuverability. In the biplane case, each wing operates at a lower wing load and cruise conditions are now reasonably far from the stall condition. Experimental measurements show that the maximum lift force is reduced when the aspect ratio is increased but that the biplane effect tends to restore the maximum lift to a level comparable to a monoplane wing of lower aspect ratio.

Naturally, a biplane configuration produces a parasite drag which amounts to about $s \cong 1.5$ times the skin friction drag of a single wing. From Eq. (14) and the definition of the mean wing chord, the skin friction drag of a monoplane wing can be expressed as

$$(D_f)_{Mo} = qgb\sqrt{\bar{c}} = qg\frac{b^{3/2}}{\sqrt{AR}} \tag{15}$$

Let us consider a biplane wing of equal maximum dimension b. To fit into a sphere of diameter b, each wing will therefore have a shorter span $b_0 = \sqrt{b^2 - G^2}$. As a result, the total skin friction drag force of a biplane wing of equal maximum size will be

$$(D_f)_{\mathrm{Bi}} = 2sqgb_0\sqrt{\bar{c}} = 2sqg\frac{b_0^{3/2}}{\sqrt{AR}} \tag{16}$$

Then, for a biplane wing of aspect ratio $AR = 2$ the skin friction drag can be related to the skin friction drag of a monoplane wing of equal maximum dimension and an aspect ratio $AR = 1$ according to

$$(D_f)_{\mathrm{Bi}} = s\sqrt{2}\beta^{3/2}(D_f)_{\mathrm{Mo}}, \qquad \beta = \frac{b_0}{b} = \frac{\sqrt{b^2 - G^2}}{b} \tag{17}$$

According to Prandtl's biplane theory [14], the total induced drag $(D_i)_{Bi}$of two identical elliptically loaded wings in biplane configuration is

Table 2 Comparison of monoplane and biplane drag forces

Case	Monoplane $AR = 1$	Monoplane $AR = 2$	Biplane $AR = 2$
Wingspan	b	b	$\sqrt{b^2 - G^2}$
Maximum dimension	B	B	B
Total lift	W	W	W
Maximum lift	L	L/D	L
Skin friction drag	D_f	$D_f/\sqrt{2}$	$s\sqrt{2}\beta^{3/2}D_f$
Induced drag	D_i	D_i	$[(\sigma+1)/2\beta^2]D_i$
total drag at constant lift	$D_f + D_i$	$D_f/\sqrt{2} + D_i$	$s\sqrt{2}\beta^{3/2}D_f + [(\sigma+1)/2\beta^2]D_i$

$$(D_i)_{Bi} = \frac{\sigma+1}{2}\frac{W^2}{\pi q b_0^2} = \frac{\sigma+1}{2\beta^2}(D_i)_{\text{Mo}} \tag{18}$$

where $(D_i)_{\text{Mo}}$ is the induced drag of a monoplane wing and σ is the interference factor defined as

$$\sigma \cong \frac{1}{1+5.3G/B} \tag{19}$$

where G is the vertical distance between the two wings. Let r be the ratio of the induced drag over the total drag in the case of a monoplane wing of aspect ratio 1

$$r = \frac{D_i}{D_i + D_f} \tag{20}$$

the ratio of the biplane total drag over the monoplane total drag of aspect ratio 1 reduces to

$$s\sqrt{2}\beta^{3/2}(1-r) + \frac{\sigma+1}{2\beta^2}r \tag{21}$$

If G/b_0 and s are fixed, the total drag at constant lift of a biplane MAV is less than a monoplane MAV of equal maximum dimension whenever

$$r \geq r_{\min} = \frac{s\sqrt{2}\beta^{3/2} - 1}{s\sqrt{2}\beta^{3/2} - (\sigma + 1/2\beta^2)} \tag{22}$$

As an example, assume $G/b_0 = 0.5$ and $s \cong 1.5$, from the definition of β and Eq. (19), one gets $\beta \cong 0.894$ and $\sigma \cong 0.274$. Finally, from Eq. (22), $r_{\min} \cong 0.796$, which means that a biplane concept yields better aerodynamic performance over the monoplane concept as soon as the induced drag of the monoplane represents at least 80% of the total drag in cruise conditions. More precisely, the ratio r can be simply related to flight conditions so as to provide numerical values to assess the benefit of the biplane concept over the monoplane wing. Combining Eq. (15) and (18), one can derive the ratio of the skin friction drag over the induced drag for a monoplane wing as

$$\left(\frac{D_f}{D_i}\right)_{\text{Mo}} = \frac{\pi h \upsilon^{1/2}\rho^2}{2}\frac{V^{7/2}b^{7/2}}{W^2} = \frac{1}{r} - 1 \tag{23}$$

Using the above numerical example, the condition expressed by Eq. (22) then reads

$$\left(\frac{D_f}{D_i}\right)_{\text{Mo}} < \frac{1}{r_{\min}} - 1 \cong 0.256 \tag{24}$$

which corresponds, according to Eq. (23), to the following condition

$$\text{biplane MAV if } \frac{V^7 b^7}{W^4 AR} < C = \frac{4(0.256)^2}{\rho^4 \pi^2 h^2 \upsilon} \tag{25}$$

where $C \cong 460\ \text{m}^{10}\,\text{kg}^{-4}\,\text{s}$ at standard conditions. Then, for a typical monoplane aspect ratio of $AR \cong 1.5$, the condition reduces to

$$\frac{V^7 b^7}{W^4} < 690 \tag{26}$$

This means that a biplane MAV is preferable when the speed and the overall size are low, and the MAV is heavily loaded, which is usually the case for practical micro air vehicles carrying sensors and navigation devices. Furthermore, stabilized video transmission requires the capability to perform low-speed flight phases. Let us consider the following typical example: $V = 10$ m/s, $b = 0.15$ m (6 in.) and $W = 0.49$ N (50 g). To sustain a steady forward flight, the cruise lift coefficient of $C_L = 0.53$ is achieved and the ratio in Eq. (26) is equal to 296, which means that the biplane concept should be selected. Yet, not all flight situations favor the biplane MAV concept over the monoplane wing. Only if strict conditions on low size and low flight speed are imposed should the biplane concept be considered. Furthermore, the threshold value C is only given here as an order of magnitude. A more accurate evaluation based on experimental calibration should be used in practice.

The weight penalties for the biplane due to an additional wing and struts can be evaluated through the following. The structural weight of an electrically powered MAV typically represents less than 20% of the total weight [1]. In the present wing-body configuration, half of the structural mass is due to the body and the other half is due to the wing. Provided that the aspect-ratio biplane wings can be greater ($AR = 2.5$) than the aspect ratio of a monoplane MAV ($AR = 1.5$), the structural mass of biplane wings amounts to

$$m_{\text{Bi}} = 2m_{\text{Mo}}\frac{AR_{\text{Mo}}}{AR_{\text{Bi}}} + m_{\text{struts}} \cong 1.2m_{\text{Mo}} + m_{\text{struts}} \tag{27}$$

that is an increase of 20%, let alone the struts mass. In a biplane configuration, the struts, which may be used as a vertical tail, and also present on a monoplane MAV, can be chosen such that its weight does not exceed half of a single biplane wing mass. Therefore, the structural mass of biplane wings can be calculated as

$$m_{\text{Bi}} = 1.2m_{\text{Mo}} + 0.3m_{\text{Mo}} = 1.5m_{\text{Mo}} \tag{28}$$

which means a 50% increase in wing structural weight when compared with a monoplane wing. Finally, the total structural weight penalty for the biplane MAV is limited to a 25% increase, and the total weight increase due to the biplane MAV configuration is only 5%.

Numerical Method

A vortex lattice method [15], modified to include viscous effects, has been used to predict the lift and drag of monoplane and biplane wings. The code TORNADO [16][‡] has been modified to include Thwaites model and Karman integral formula so that the incidence effect is incorporated into the flat-plate skin friction drag coefficient following

$$c_f = 2\left[\frac{0.45m}{5m+1} + 0.09\right]^{0.62}\sqrt{\frac{\upsilon \times (5m+1)}{0.45 \times k}}\frac{1}{(\sqrt{x})^{m+1}} \tag{29}$$

where x is the streamwise distance between the leading edge and the current station and

$$m = \frac{1}{1 + 2\pi/\alpha} \tag{30}$$

Form drag and interference drag are approximated by taking half of the total skin friction drag [17].

A total of 64 sweepback wings which all fit into a 20 cm-diameter disk were compared in terms of lift-to-drag ratio. Figure 5 illustrates the influence of aspect ratio on the lift-to-drag ratio and compares monoplane, biplane, and triplane wings, including induced drag and viscous drag.

For a given aspect ratio, the biplane configuration only slightly improves the lift-to-drag ratio. This is due to the fact that the wetted area is now doubled and the minimum drag for a high aspect-ratio biplane is greater than the one associated with a monoplane of aspect ratio 1. Naturally, the lift is not doubled when doubling the wings because of unfavorable interaction between them. Yet, because of a lower induced drag, the biplane configuration is still better than the monoplane wing with an identical aspect ratio and that of the monoplane with aspect ratio 1. Also, a desirable value of aspect ratio of 2 to 3 can be selected to design a biplane MAV. Finally, a triplane configuration of aspect ratio 4 was also calculated and plotted (diamonds on Fig. 5). Its lift-to-drag ratio is lower than in the case of biplane configurations because of excessive parasite drag. The triplane configuration, although acceptable for flight, is not better than a biplane with lower aspect ratio.

[‡]See http://www.flyg.kth.se/divisions/aero/software/tornado/ [cited 17 December 2005].

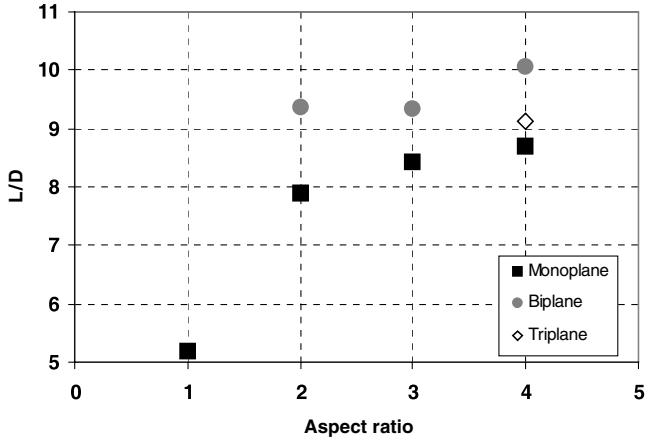

Fig. 5 Lift-to-drag ratio of monoplane, biplane, and triplane wings.

Table 3 compares three configurations of equal maximum dimension: a) a monoplane square wing of aspect ratio 1, b) a monoplane rectangular wing of aspect ratio 2, c) a biplane wing of aspect ratio 2. All three wings fit into a 20 cm-diameter disk so that the span is not constant in the present calculation. Stall lift values were obtained from wind-tunnel measurements whereas cruise values were computed through the vortex-lattice method corrected with viscous effects. For a given maximum overall size and a fixed lift force at cruise conditions, a biplane concept provides lower drag (35% reduction) by drastically reducing the induced drag while increasing the parasite drag by 80%. Stall lift force does not significantly benefit from the biplane concept with only a slight increase of 6% in maximum lift, although further optimization is certainly needed here, especially by staggering the wings. Finally, computed cruise lift-to-drag ratio can be increased by 53% when using a biplane wing. In practice, parasite drag due to struts partially degrades the biplane lift-to-drag performance.

Experimental Measurements

Experimental measurements have been carried out on a series of monoplane and biplane wings which all fit into a 20-cm-diameter disc. All three wing configurations are compared at the same cruise condition when $C_L \cong 0.42$. As shown on Table 4, increasing the aspect ratio from 1 to 2 on a monoplane Zimmerman wing dramatically reduces the induced drag and significantly improves the maximum lift-to-drag ratio as well as the cruise lift-to-drag ratio. However, the maximum lift coefficient is strongly affected by the increase in aspect ratio of a monoplane wing. Table 4 also illustrates the fact that a biplane configuration can nearly retrieve the maximum lift of a monoplane wing of equal surface and span. Some optimized biplane configurations can even provide a greater maximum lift than for a monoplane wing of equal surface and span. Finally, a MAV biplane configuration can produce a much higher lift-to-drag ratio at cruise conditions. Using the inverse Zimmerman wing planform, the same comparison between monoplane wings (InvZim1, $AR = 1$ and InvZim2, $AR = 2$) and a biplane wing (BiInvZim, $AR = 2$) can be made. Figure 6 confirms that the biplane concept (BiInvZim, $AR = 2$) becomes attractive for a fairly high cruise lift coefficient because of the induced drag reduction associated with the biplane effect. It should be noticed that the maximum lift can be further improved in the case of biplane wings by propeller-induced flow which delays stall. Therefore biplane wings not only improve the aerodynamic performance in cruise conditions but are also potentially superior in terms of maneuverability.

Table 4 Aerodynamic performance of monoplane and biplane wings

Wing configuration	Λ	$C_{D\,\min}$	k	$C_{L\,\max}$	$L/D_{(\text{cruise})}$	$L/D_{(\max)}$
Monoplane	1	0.055	0,54	1.25	3.89	4.04
Monoplane	2	0.042	0,33	0.59	4.38	5.11
Biplane	2	0.066	0,27	1.06	5.19	5.48

Optimization of Biplane MAVs

Biplane wings can be arranged in various ways to produce different aerodynamics effects. Three parameters are classically considered: gap, stagger, and decalage angle. The gap is the vertical distance between both wings. The stagger [18] is the horizontal distance, counted positive if the lower wing is located downstream of the upper one. The decalage angle [19] is the angle of attack of the upper wing with respect to the lower wing chord. Experimental measurements were carried out on a biplane configuration using two identical Zimmerman wings, and a tandem configuration using one Zimmerman wing and one inverse Zimmerman wing. All wings are based on the curved-plate *Göttingen 417a* wing section and have a maximum dimension of 20 cm. Both wings are attached by using four cylinders of diameter 0.8 mm. Gap, stagger, and decalage angle can be adjusted.

On Fig. 7, three different gap distances have been compared: 3, 5, and 7 cm without stagger. It can be observed that a higher gap yields a slightly higher lift force gradient and higher maximum lift. However, the stall incidence is accordingly slightly reduced when the gap is increased. Yet, drag measurements indicate that increasing the gap does not affect the wing maximum lift-to-drag ratio. Indeed, as the parasite drag is increased for the biplane wings, the induced drag factor is lowered. The parasite drag of cylinders increases with the gap, particularly at low Reynolds numbers where interference drag is significant. Gap also increases the maximum dimension of model, it is not beneficial to choose a gap greater than a wing chord. In the following, a value of 5 cm—to be compared with a mean chord value of 8.7 cm—has been chosen to study the other geometrical parameters. This relatively small value has also been selected in order to satisfy the overall maximum dimension constraint.

Stagger effect has been studied for a fixed gap distance of 5 cm using 3 different values of positive stagger: 2, 4, and 6 cm (referred to as S2, S4, and S6, respectively, on the diagram). In addition, two tandem wings configurations have been investigated. "tandem SP" (TSP) refers to a configuration where the upper wing is an *inverse* Zimmerman planform wing located upstream a Zimmerman planform wing with a maximum *positive* stagger of 7.5 cm "tandem SN" (TSN) is a configuration where the upper wing is a Zimmerman planform wing placed downstream an inverse Zimmerman planform wing with a *negative* stagger of 7.5 cm. For both tandem wing configurations, the whole model fits into a 20-cm-diameter sphere. By contrast to higher Reynolds-number aerodynamic configurations [18], a positive stagger slightly increases the lift slope at low-Reynolds regime and the maximum lift is significantly increased (Fig. 8a). The highest value of the maximum lift coefficient is obtained for the "TSP" configuration which corresponds to a positive stagger of 7.5 cm. Also, the upper wing stalls earlier when stagger is positive. This can be explained by the fact that the upwash angle due to the lower wing artificially increases the angle of attack

Table 3 Comparison of rectangular monoplane and biplane wings

AR	chord (cm)	span (cm)	Concept	$L_{\max}$ (g.) exp. data	Cruise (at 10 m/s, weight 80 g.)						
					α (deg)	L (g.)	D_t (g.)	D_0 (g.)	D_i (g.)	L/D	D_i/D_t
1	14.1	14.1	Monoplane	148.5	19.0	80	13.5	1.9	11.6	5.93	85.9%
2	8.9	17.8	Monoplane	96.0	14.4	80	10.1	1.7	8.4	7.89	83.1%
2	8.9	17.8	Biplane	158.3	9.5	80	8.7	3.4	5.3	9.13	60.8%

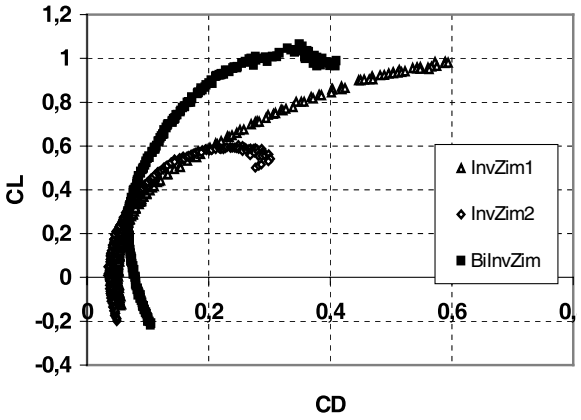

Fig. 6 Comparison of drag polars: InvZim1 ($Re = 126,000$), InvZim2 and BiInvZim2 ($Re = 66,000$).

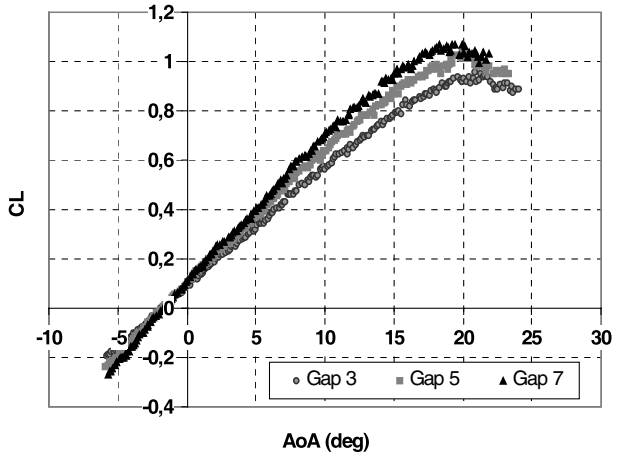

Fig. 7 Gap effect: $Re = 66,000$.

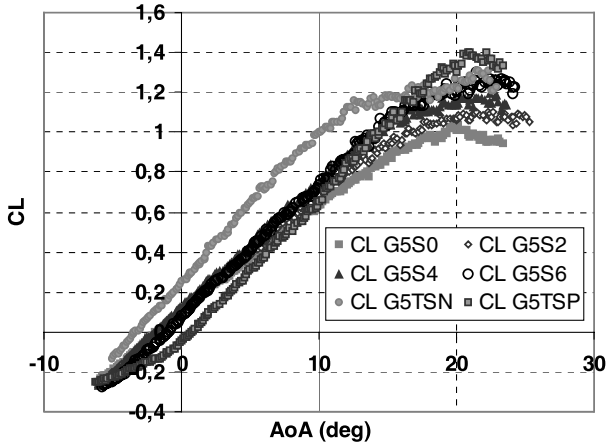

a) Lift coefficient

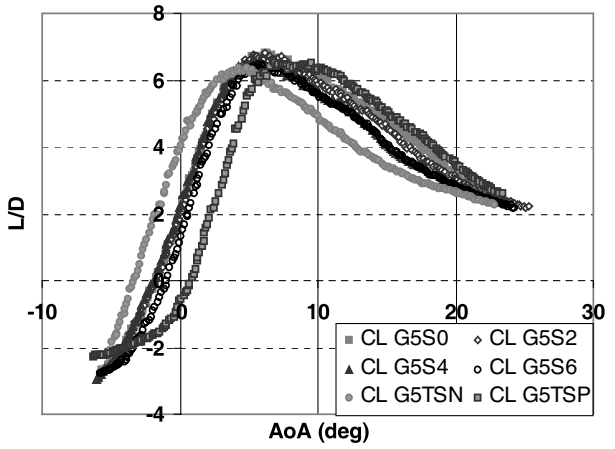

b) Lift-to-drag ratio

Fig. 8 Influence of the stagger effect. Vertical distance between biplane wings is 5 cm: $Re = 66,000$.

on the upper wing. Yet, the maximum lift-to-drag ratio is roughly the same for various stagger values (Fig. 8b).

Table 5 summarizes the different combination effects: 1) increasing the vertical distance between biplane wings is only slightly beneficial to the lift-to-drag ratio, both at cruise conditions and at maximum lift-to-drag ratio. Yet, it also increases the total weight due to higher struts. Furthermore, in order to maintain a constant maximum dimension $B = \sqrt{b^2 + G^2}$, the biplane wingspan must be reduced. Note that this maximum dimension effect is not accounted for in Table 5; 2) a positive stagger improves the maximum lift coefficient and accordingly increases the MAV flight envelope. Yet, because the overall MAV configuration must stay within a 20-cm-diameter sphere, stagger increase eventually implies a total wing surface reduction, 3) because tandem wings make the most of the available wing surface, they both yield high maximum lift-to-drag ratios. The negative staggered tandem configuration (TSN) can even reach a maximum lift-to-drag ratio close to 6 but is less attractive in terms of maximum lift coefficient.

As a conclusion, a significant amount of positive stagger—typically $\frac{1}{3}$ of the wingspan (which corresponds to a stagger of 7 cm on Table 5) is desirable for biplane MAVs because it dramatically increases the maximum lift force while not degrading the lift-to-drag ratio. Using an inverse Zimmerman planform as a front wing (TSP), which takes full advantage of the maximum allowable area, high performance and high stall lift can be obtained. Yet, stall may be strongly affected by the flow induced by propellers, as will be observed in the next section.

Propeller Effect

Propeller-driven MAVs are strongly affected by the propeller-induced flow [20]. This is due to the fact that propeller efficiency rapidly drops when the diameter is reduced. As a consequence, the propeller diameter should be maximized and usually represents a large portion the wingspan. Furthermore, at low-Reynolds numbers, the propeller-induced flow can help delay stall. In this section, wind-tunnel measurements have been performed to measure the effect of the motor-propeller position. A biplane MAV model based on the "tandem SP" configuration has been made out of two 2 mm-thick aluminum flat plates in order to minimize the effect of vibrations due to the motor. The investigation has been done in the low-speed wind tunnel described above. The longitudinal aerodynamics characteristics were observed from an angle of attack -10 deg to stall angle.

Three different propeller positions have been considered: the "LE-for" leading edge fore-wing position (Fig. 9a), the "TE-for" trailing edge fore-wing position (Fig. 9b) and the "LE-aft" leading edge aft-wing position. Additional investigations showed that intermediate motor positions only degraded the overall performance. A DC coreless *Maxon* motor of 10 g was used to drive a 8 cm-diameter

Table 5 Aerodynamic performance of biplane wing combinations

Biplane wing combination	$C_{D\,\min}$	k	$C_{L\,\max}$	$L/D_{(\text{cruise})}$	$L/D_{(\max)}$
Gap 5 cm	0.066	0.27	1.06	5.19	5.48
Gap 7 cm	0.066	0.26	1.09	5.45	5.81
Stagger 4 cm	0.066	0.25	1.21	5.53	5.82
Stagger 7 cm	0.066	0.24	1.32	5.53	5.81
Tandem SP	0.067	0.23	1.42	5.25	5.80
Tandem SN	0.067	0.23	1.33	5.12	5.97

a) Leading-edge fore-wing

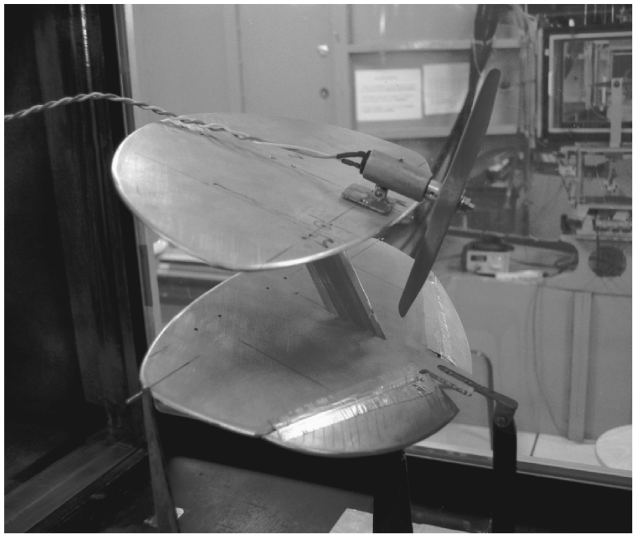

b) Trailing edge fore-wing

Fig. 9 Propeller position effect.

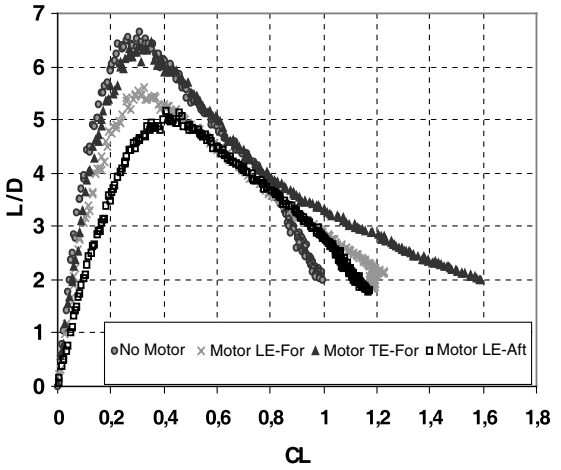

Fig. 10 Effect of propeller position.

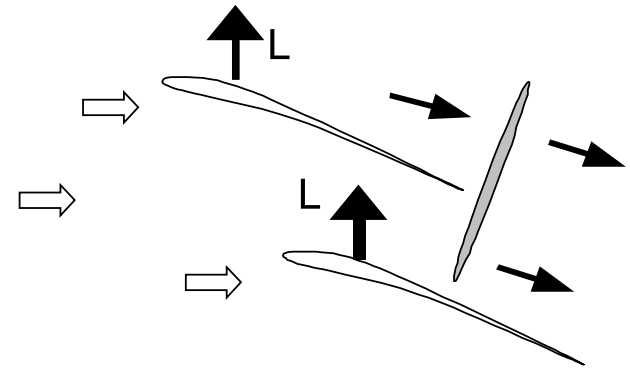

a) Trailing edge fore-wing position

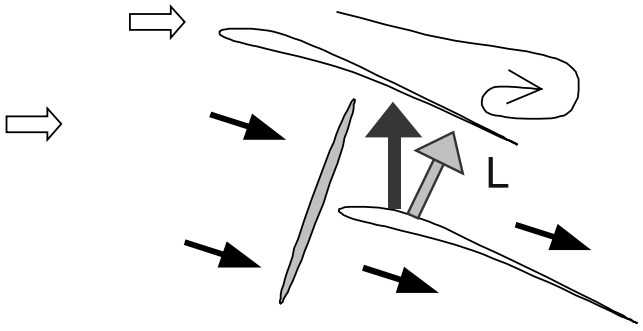

b) Leading edge aft-wing position

Fig. 11 Propeller-induced flow: effect of propeller location.

propeller under 6 Volts with an average current of 1.2 A. As illustrated on Fig. 10, the trailing edge fore-wing position has the advantage of maintaining a high value of maximum lift-to-drag ratio while dramatically increasing the maximum lift. Model's maximum lift coefficient of 1.0 by no-motor-propeller configuration is improved to 1.6 by an optimal-motor-position configuration. This motor position is also interesting for practical reasons because it protects the propellers during landing. This optimal position can be explained by the fact that the flow induced by the propeller delays the stall both on the upper wing and the lower wing (Fig. 11a). On the other hand, when the propeller is located on the leading edge (either on the upper wing or the lower wing), the stagnation point is moved upward and the circulation is reduced so that the wing lift-to-drag ratio decreases. Furthermore, in the "LE-aft" configuration, the leeward side of the upper wing receives very little aerodynamic influence from the propeller (Fig. 11b).

Finally, the motor's setting angle could be adjusted using positive or negative angles at each motor position. It was observed that the setting angle has very little influence on aerodynamic performance.

Conclusions

The present study showed the benefit of using a biplane wing instead of the classical monoplane wing if the overall dimension is fixed within the range of MAV dimensions. Because biplane wings can sustain level flight with higher aspect-ratio wings, the biplane induced drag force is lower than when using monoplane wing for a given lift force. This conclusion is strongly related to the fact that MAV wings are strictly constrained in overall dimension and weight. Although the parasite drag is significantly increased for a biplane wing, the fact that monoplane MAVs usually operate with low aspect-ratio wings makes higher aspect-ratio biplane wings more attractive. Both experimental and numerical approaches confirm that a biplane wing has more aerodynamic efficiency than a monoplane wing at the same flight conditions, provided that low-speed, heavy-load, and small-size conditions are required. The present conclusions are consistent with recent low-speed experimental studies carried out on biplane delta wings [21]. Wings combination effects, including gap and stagger effects, show that an optimized configuration consists of two highly staggered wings based on Zimmerman and

inverse Zimmerman planforms. Furthermore, the propeller-induced flow is highly beneficial to the maximum lift when the motor is placed near the upper wing trailing edge. This tandem wing configuration also allows for compensating the nose-down pitching moment by using a positive decalage angle. The effect of a positive decalage angle for a tandem wing configuration in terms of performance is comparable to the effect of an inverse camber for flying wing MAVs. Another alternative would consist of adding a horizontal tail downstream. It should be noticed that because biplane wings allow for higher aspect ratios ($AR \cong 2.5$), a wing-tail configuration is now possible although it is more difficult to achieve for a classical monoplane MAV limited to a lower aspect ratio ($AR \cong 1.5$).

Acknowledgments

The present work is supported by the French Ministry of Defence, under Grant No. DGA-036000070. This study could not have been completed without the constant support from the Composite Material Laboratory of SUPAERO where all models were fabricated. The author would like to express their gratitude to Alain Combes and Paul-Claude Dufour for their assistance to produce the present wind-tunnel measurements and to all members and students of the Aerodynamics Laboratory of SUPAERO for their helpful discussions and contributions to the present study.

References

[1] Grasmeyer, J. M., and Keennon, M. T., "Development of the Black Window Micro Air Vehicle," *Fixed and Flapping Wing Aerodynamics for Micro Air Vehicle Applications*, edited by T. J. Mueller, Vol. 195, Progress in Astronautics and Aeronautics, AIAA, Reston, VA, 2001, pp. 519–535.

[2] Torres, G. E., and Mueller, T. J., "Aerodynamics Characteristics of Low-Aspect Ratio Wings at Low Reynolds Numbers," *Fixed and Flapping Wing Aerodynamics for Micro Air Vehicle Applications*, edited by T. J. Mueller, Vol. 195, Progress in Astronautics and Aeronautics, AIAA, Reston, 2001, pp. 115–141.

[3] Torres, G. E., and Mueller, T. J., "Low-Aspect-Ratio Wing Aerodynamics at Low Reynolds Numbers," *AIAA Journal*, Vol. 24, No. 5, 2004, pp. 865–873.

[4] Pelletier, A., and Mueller, T. J., "Low Reynolds Number Aerodynamics of Low-Aspect-Ratio, Thin/Flat/Cambered-Plate Wings," *Journal of Aircraft*, Vol. 37, No. 5, 2000, pp. 825–832.

[5] Lyon, C. A., Broeren, A. P., Giguere, P., Gopalarathnam, A., and Selig, M. S., *Summary of Low-Speed Airfoil Data*, Vol. 3, SoarTech Publications, Virginia Beach, 1998, p. 128.

[6] Thipyopas, C., and Moschetta, J. M., "Improved Performance of Micro-Air Vehicles Using Biplane Configuration," *11th Australian International Aerospace Congress, Melbourne, Australia* [CD-ROM], Paper WC0120, March 2005.

[7] Zimmerman, C. H., "Characteristics of Clark Y Airfoils of Small Aspect Ratios," NACA TR 431, May 1932.

[8] Suhariyono, A., Kim, J. H., Goo, N. S., Park, H. C., and Yoon, K. J., "Design of Precision Balance and Aerodynamic Characteristic Measurement System for Micro Aerial Vehicles," *Aerospace Science and Technology*, Vol. 10, No. 2, 2006, pp. 92–99.

[9] Kochersberger, K., and Abe, C., "A Novel, Low Reynolds Number Moment Balance Design for Micro Air Vehicle Research," AIAA Paper 2005-4759, June 2005.

[10] Barlow, J. B., Rae, W. H., and Pope, A., *Low-Speed Wind Tunnel Testing*, 3rd ed., John Wiley & Sons, New York, 1999, pp. 368–372.

[11] Kuethe, A. M., and Chow, C.-Y., *Foundations of Aerodynamics, Bases of Aerodynamic Design*, 5th ed., John Wiley & Sons, New York, 1998, p. 374.

[12] Viieru, D., Albertani, R., Shyy, W., and Ifju, P. G., "Effect of Tip Vortex on Wing Aerodynamics of Micro Air Vehicles," *Journal of Aircraft*, Vol. 42, No. 6, 2005, pp. 1530–1536.

[13] Rais-Rohani, M., and Hicks, G. R., "Multidisciplinary Design and Prototype Development of a Micro Air Vehicle," *Journal of Aircraft*, Vol. 36, No. 1, 1999, pp. 227–234.

[14] Prandtl, L., "Induced Drag of Multiplanes," NACA TN-182, March 1924.

[15] Katz, J., and Plotkin, A., *Low-Speed Aerodynamics from Wing Theory to Panel Methods*, McGraw–Hill, Singapore, 1991.

[16] Melin, T., "A Vortex Lattice Matlab Implementation for Linear Aerodynamics Wing Applications," Master Thesis, Department of Aeronautics, Royal Institute of Technology, Stockholm, Sweden, 2000.

[17] Jobe, C. E., "Prediction and Verification of Aerodynamic Drag, Part 1: Prediction," *Thrust and Drag: Its Prediction and Verification*, edited by E. E. Covert, Vol. 98, Progress in Astronautics and Aeronautics, AIAA, New York, 1985, p. 131.

[18] Norton, F. H., "The Effect of Staggering a Biplane," NACA TN-70, September 1921.

[19] Mock, R. M., "The Distribution of Loads Between the Wings of a Biplane Having Decalage," NACA TN-269, November 1927.

[20] Null, W., Nosek, A., and Shkarayev, S., "Effects on Propulsive-Induced Flow on the Aerodynamics of Micro Air Vehicle," AIAA 2005-4616, June 2005.

[21] Traub, L., "Theoretical and Experimental Investigation of Biplane Delta Wings," *Journal of Aircraft*, Vol. 38, No. 3, 2001, pp. 536–546.